Cement and Concrete Research 90 (2016) 19–26

Contents lists available at ScienceDirect

Cement and Concrete Research

journal homepage: www.elsevier.com/locate/cemconres

Effect of electrical field on TSA failure of cement-based materials

Yaoling Luo, Chong Wang *, Chaoqun Luo, Qian Huang, Shupin Wang, Xiaoqin Peng

College of Materials Science and Engineering, Chongqing University, Chongqing 400045, China

ARTICLE INFO

Article history:
Received 19 February 2016
Received in revised form 12 September 2016
Accepted 12 September 2016
Available online 19 September 2016

Keywords:
Electrical field
Cement-based materials
TSA

ABSTRACT

The impact of electrical field on the sulfate attack of cement-based materials at low temperatures was studied to rapidly detect Thaumasite Sulfate Attack (TSA) in the laboratory and in future engineering. Sulfate attack of cement paste with 30 wt% replacement of $CaCO_3$ powder soaked in Na_2SO_4 solution, $MgSO_4$ solution, or $CaSO_4$ solution was measured under the condition of 5 ± 2 °C when an electrical field was applied. Appearance changes and compressive strength of the samples were tested to evaluate the corrosion degree. Scanning Electron Microscopy (SEM), X-ray Diffraction (XRD), Fourier Transform Infrared Spectroscopy (FTIR) and Raman Spectroscopic measurements were applied to study the microstructure of the corrosion product. The test results indicate that sample damage was obvious, compression strength declined rapidly, and ettringite and/or thaumasite were found in the corrosion product after applying the electrical field for 90 days. A muddy product with TSA characteristics was formed, and thaumasite composition was found in the corrosion product after applying the electrical field for 120 days when $MgSO_4$ solution was used as the corrosion medium. It is confirmed that an electrical field can accelerate TSA failure in cement-based materials.

1. Introduction

The influence of electrical fields on concrete, e.g., the stray current produced by urban rail transit, has been gradually recognized in engineering. The traction of urban rail transit is DC power, and steel railing has significant resistance, leading to the potential difference in the steel rail and the potential difference between the steel rail and concrete roadbed. The electric current that transfers into the concrete is called stray current. These corrosion problems have been discovered in Beijing and Tianjin in China and in Japan and America [1]. Concrete structures can also be corroded by sulfate from the soil, groundwater, and seawater in these regions. Moreover, concrete can be influenced by electrical fields produced by the electro-osmosis pulse used for water-proofing and damp-proofing [2,3]. Electro-osmosis pulse has been successfully applied for water-proofing and damp-proofing of concrete; however, when sulfates are present in the soil and groundwater, concrete will be corroded by the electric field and sulfate attack. Nevertheless, scholars have focused on the electrochemical corrosion of reinforcement in concrete [4–7] by electrical fields, ignoring the influence of electricity on cement. In particular, concrete is more easily corroded in cold regions, producing thaumasite [8,9]. Therefore, concrete is subject to more serious damage in the presence of an electrical field.

The durability of concrete may degrade through use for internal and external reasons, which has economic consequences for countries. Moreover, this degradation also increases potential risk [10]. Sulfate attack to concrete is the most sophisticated type of corrosion. Sulfate from soil and ground water can react with the cement, which results in the expansion, cracking and spalling of concrete [11]. Thaumasite Sulfate Attack (TSA) is one corrosion mechanism of sulfate attack that was discovered in recent decades and has attracted increasing attention from researchers [12–14]. TSA is a special form of corrosion of cement-based materials that occurs naturally in minerals of the type $CaSiO_3 \cdot CaSO_4 \cdot CaCO_3 \cdot 15H_2O$ and has been found in metamorphosed rocks that have undergone hydrothermal changes over time. Thaumasite is a pulp without bonding capabilities that contributes to the destruction of concrete construction [15,16]. The formation rate of thaumasite is usually decades in nature [17]. However, thaumasite can be rapidly produced within 6 months to 2 years in the laboratory by soaking in magnesium sulfate solution or inner-introduced sulfate at low temperatures [18,19]. The long period required to form thaumasite is a disadvantage in the laboratory and in some real-world detection tests. Therefore, it is necessary to research the sulfate attack of cement-based materials under electrical field conditions, which can not only accelerate the study of TSA as a method for testing quickly TSA in laboratory, but can also provide insight into the deterioration mechanism of concrete exposed to an electrical field and sulfate in engineering.

The aim of this paper is to study the acceleration rates of three types of sulfates (Na_2SO_4 solution, $MgSO_4$ solution and $CaSO_4$ solution) under

* Corresponding author.
E-mail addresses: 504360595@qq.com (Y. Luo), chongwang@cqu.edu.cn (C. Wang).

http://dx.doi.org/10.1016/j.cemconres.2016.09.011
0008-8846/

an electrical field and the mechanism of sulfate and electrical corrosion of cement-based materials.

2. Materials and methods

2.1. Preparation of basic materials

Grade 42.5R of ordinary Portland cement composed with 97wt% clinker and 3wt% dihydrate gypsum were prepared. The chemical components of the cement clinker are listed in Table 1. Limestone powder with $CaCO_3$ ≥98 wt% was obtained from Bao Xing Company, Sichuan province China. The XRD of the cement clinker and limestone powder are presented in Fig. 1 and Fig. 2.

2.2. Specimen preparation

Cement paste was prepared to test thaumasite formation via the action of an electrical field. The mixture proportions are listed in Table 2.

The fresh paste was casted into a PMMA mould with three cube specimens with dimensions of 40 mm × 40 mm × 40 mm, which have two end containers for the sulfate solution. The specimens, together with the mould, were cured for 28 days in a moist room at a temperature of (20 ± 2) °C with a relative humidity of no less than 95% until testing. After curing, the specimens, together with the mould, were moved into a refrigerating cabinet with a temperature of 5 ± 2 °C (shown in Fig. 3 [20] and Fig. 4). Two titanium alloy staffs were used as the anode and cathode materials, respectively. An electrical field was applied to accelerate the migration of sulfate ions into the cement-based materials. The electrical voltage was 30 V, and the period was 20 s. The waveform of electrical pulses is shown in Fig. 5 [20].

All cathode solutions were Na_2SO_4 solutions. The anode solutions were Na_2SO_4 solution (EFN), $MgSO_4$ solution (EFM), and $CaSO_4$ solution (EFC). The control group consisted of samples fully immersed in $MgSO_4$ solution (M); the SO_4^{2-} concentration of the four groups of sulfate solutions was 0.38 mol/l, and the solution was replaced every 7 days. Samples fully immersed in $MgSO_4$ solution were denoted as the control group because $MgSO_4$ can promote thaumasite sulfate attack of cement-based materials. The research results of Hobbs DW [21] showed that magnesium ions and the formation of insoluble $Mg(OH)_2$ can reduce the pH and increase the degree of chemical attack on C–S–H, thus playing a major role in increasing the occurrence of thaumasite attack. The acceleration of thaumasite formation (TF) in $MgSO_4$ solution was also confirmed by Zanqun Liu [22]. Moreover, additional studies [23,24] have used $MgSO_4$ solution to research the thaumasite sulfate attack of cement-based materials.

According to the principle of electrochemistry, water was electrolyzed on the electrode and electrolysis cannot happen within the cement sample. The process of water electrolysis is as follows:

$$\text{Cathode}: 4H_2O + 4e^- = 2H_2(g) + 4OH^-(aq) \quad (1)$$

$$\text{Anode}: 2H_2O = O_2(g) + 4H^+(aq) + 4e^- \quad (2)$$

The corrosion liquid of the cathode is basic, and the corrosion liquid of the anode is acidic under an electrical field. Moreover, the anion will migrate from the cathode to the anode under the action of an electrical field. Therefore, SO_4^{2-} migrates from the cathode to the anode, leading to the accumulation of SO_4^{2-} on the cathode side of the sample [20,25–28]. The sulfate attack of cement usually occurs in an alkaline environment, and the abundance of SO_4^{2-} in the cathode leads to the acceleration of TSA in the cathode, while mainly ionic migration and acid corrosion occur in the anode.

These samples were observed every 30 days, and the damage grades were judged according to Table 3 [24] until failure character of TSA was occurred in these samples. Then, micro samples were created for XRD, SEM, and EDS tests. FTIR was used to identify the microstructure of thaumasite formation. The samples for the analysis of thaumasite formation were produced by taking small pieces from the cathode side of the attacked specimen. The broken pieces were soaked and rinsed using anhydrous alcohol and oven dried at 50 °C. The X-ray diffractometer used was from Ricoh Company with D/MAX-IIIC and CoKα radiation (0.2 Å). VEGA II SEM instrument with EDS was from Tescan Company. The SEM investigation was carried out using an accelerating voltage of 20 kV. Fourier Transform Infrared Spectroscopy (FTIR) instrument with a resolution of 4 was used. Raman spectroscopic measurements were carried out using a HORIBA Jobin Yvon S.A.S. spectrometer (product model: LabRAM HR Evolution; spectral resolution: visible spectral ≤0.65 cm^{-1}; spectral region from 200 nm to 1050 nm).

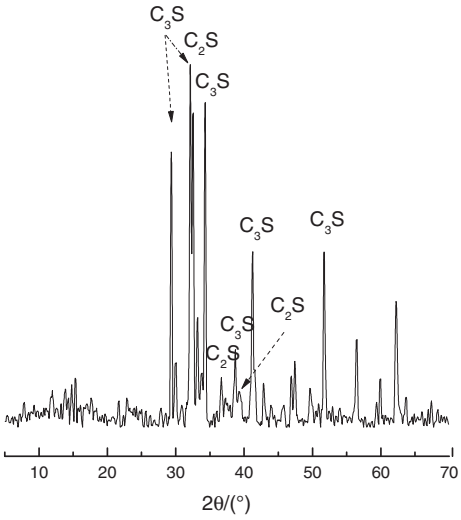

Fig. 1. XRD of cement clinker.

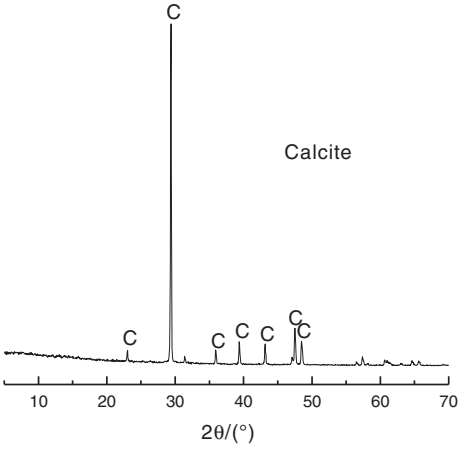

Fig. 2. XRD of limestone powder.

Table 1
Chemical components of clinker, dihydrate gypsum, and limestone powder (wt%).

Materials	SiO_2	Fe_2O_3	Al_2O_3	CaO	MgO	SO_3	K_2O	Na_2O	LOI
Clinker	19.99	2.98	4.80	61.22	3.27	0.23	0.88	0.18	3.52
Gypsum	4.47	0.36	0.99	34.05	1.84	40.61	0.23	0.08	16.87
Limestone powder	0.23	0.21	–	55.46	–	–	–	–	41.75

Table 2
Mixture proportions of cement paste.

Cementitious materials (wt%)		Water/cementitious materials ratio
Cement	$CaCO_3$ powder	
70	30	0.40

3. Results and discussion

3.1. Appearance of samples

The appearance of the samples after the action of an electrical field for 120 days is presented in Fig. 6. The four samples were visibly damaged, presenting cracking and spalling after 90 days. The EFM was damaged and presented the typical characteristics of TSA, producing significant amounts of pulp after 120 days. However, this was not observed in the other three samples. There was an obvious accelerating process from 90 days to 120 days in EFM.

The change of appearance in the samples between 90 days and 120 days is presented in Figs. 7 and 8. EFM not only showed the most serious corrosion in 90 days but also formed pulp that was similar to thaumasite after 120 days, while the other three groups did not present pulp. Meanwhile, the sulfate attack in the cathode conforms with the theoretical analysis described above.

3.2. Compressive strength

The compressive strengths of the four samples are presented in Fig. 9, and the calculation of the trim size of the compressive strength follows. The EFM samples had been destroyed in 120 days that cannot be tested for compressive strength, so the compressive strengths were tested till 90 days. The compressive strengths of the electrical field samples decline sharply from 50 MPa to less than 20 MPa within 90 days. EFM and EFC are especially affected by the electrical field after 30 days. The compressive strength of EFM is the lowest among these samples due to the dual corrosion effects of sulfate and magnesium. The compressive strengths of the samples rapidly decline, in line with the appearances of the samples within 90 days. SO_4^{2-} ions migrate continuously from the cathode solution to the interior of cement-based materials and react with $Ca(OH)_2$ and tricalcium aluminate hydrate to form ettringite, leading to expansion and microcrack formation in the samples. Moreover, H^+ ions in the anode from water electrolysis migrate into the cement, which combine with OH^- to free Ca^{2+}; Mg^{2+} and Ca^{2+} migrate to the cathode, causing the cement sample be imbalanced and affording more reactants to form ettringite, which reduces the compressive strength significantly. These above processes lead to the deterioration of the compressive strength and appearance of the samples.

The corrosion of EFM was the most serious in the four groups due to both sulfate attack and magnesium salt attack during the exposure of the cement-based materials to $MgSO_4$ solution. Additionally, compared with M, EFM corrosion was also more serious, indicating that the electrical field could accelerate the corrosion process by accelerating the migration of aggressive ions from the solution to the samples. The corrosion of EFC was the second most serious after 90 days and is more serious than that of EFN. More Ca^{2+} ions migrate from the anode $CaSO_4$ solution to the samples, and abundant SO_4^{2-} ions migrate from the cathode to the samples, leading to the formation of greater amounts of $CaSO_4$ than EFN. $CaSO_4$ converts to $CaSO_4 \cdot 2H_2O$ after absorbing water, which would expand within the samples and lead to a lower compressive strength than EFN. The results of the compressive strength and appearance indicate that the electrical field can accelerate the corrosion process.

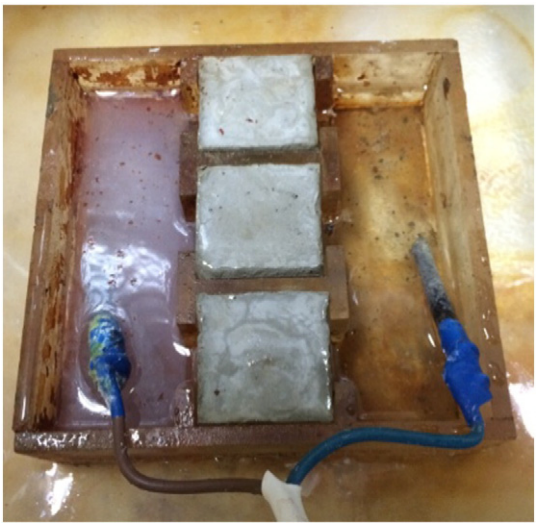

Fig. 4. Schematic diagram of the electrode.

Fig. 3. The test setup of TSA formation via the action of electrical pulses in a refrigerating cabinet.

3.3. SEM/EDS

The EFM under the action of the electrical field for 120 days was examined using SEM/EDS to identify its microstructure and elemental distribution. The SEM/EDS sample was taken from the pulp of EFM. The test

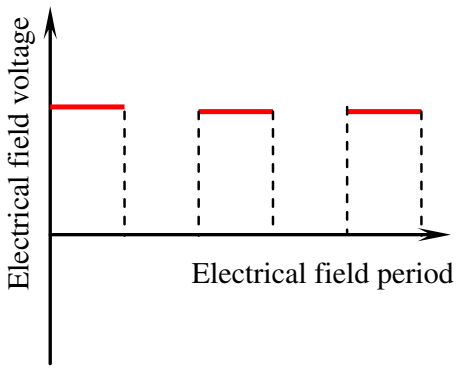

Fig. 5. Oscillogram of electrical field.

Table 3
Corrosion damage grades of TSA.

Damage grades	Corrosion features
1	No visible deterioration
2	Some deterioration at corners
3	Deterioration at corners and the edges
4	Deterioration at corners and some cracking along the edges
5	Cracking and expansion along the edges
6	Serious cracking and expansion
7	Spalling and expansion of surfaces
8	Grey pulp at corners, the edges and surface
9	Amount of grey pulp at samples
10	Complete damage

results are shown in Fig. 10 and indicate that there are large amounts of needle crystals existing in the cement-based materials. The tests identified the needle crystals as thaumasite, and the composition is found to be C, S, Si, Ca, and O, which is characteristic of thaumasite. No Al was detected. Therefore, it can be preliminarily concluded that the soft mushy incohesive mass is the thaumasite product, but more XRD, FTIR, and Raman spectroscopic evidence is required to identify the thaumasite.

3.4. XRD

XRD was conducted to further affirm thaumasite formation, and the test results after 90 days are shown in Fig. 11. These XRD samples were taken from the 2 mm cathode surface layer of the four groups. As shown in Fig. 11, the corrosion mainly contains ettringite and (or) thaumasite except for hydration products. The M group presents small mixtures of ettringite or thaumasite. In addition, the same corrosion products as in the other electrical field groups were observed but with stronger diffraction peaks. In the three electrical groups, the characteristic peak of ettringite or thaumasite can be seen (d = 3.840 Å) in EFC. The corrosion of EFN is mainly ettringite (d = 9.73 Å), and EFM had the most obvious characteristic peak of thaumasite (d = 9.553, 5.516, 3.808 Å), which indicated that there was more thaumasite in the EFM.

White precipitates are observed to dissolve out from the anode surface of the samples under the action of the electrical field. These precipitates and the XRD patterns are presented in Fig. 12. These precipitates, as analysed by XRD, are gypsum. The anode solution is acidic when electrolyzed, as shown in the above chemical Eq. (2). Ca^{2+} would be leached from the sample in an acidic environment; meanwhile, the anode solution has an amount of SO_4^{2-}, which leads to the generation of gypsum and gypsum is insoluble in acid.

Fig. 13 shows the XRD test results of corrosions from the 2 mm cathode and anode surface layers of EFM after 120 days. There are obvious characteristic peaks of thaumasite on the surface of the cathode, and they affirm that the pulp is thaumasite. Meanwhile, the electrical field not only accelerates the formation rate of thaumasite but also accelerates the formation rate of gypsum in the cathode of the sample. $Ca(OH)_2$ is exhausted to generate gypsum, which is essential to the formation of thaumasite. The presence of gypsum plays a key role in the formation of thaumasite. On the contrary, similar peaks exhibit slight deviations from the thaumasite peaks in the anode of the sample, indicating these should belong to ettringite. Moreover, the peaks of $Ca(OH)_2$ are very obvious and the peaks of gypsum are weaker than that of the cathode, indicating that the corrosion reaction process of the anode is slower than that of the cathode and there is no TSA in the anode.

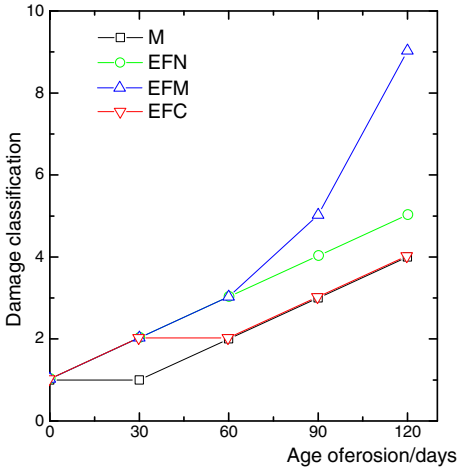

Fig. 6. Appearance change grade of samples under the corrosion condition after 120 days.

Cement-based materials will react with $MgSO_4$ to $Mg(OH)_2$ as shown in reaction (3), which is difficult to dissolve in water when the aggressive medium is $MgSO_4$. However, reversible chemical reaction (4) occurs without magnesium salt [22,29].

$$Ca(OH)_2 + MgSO_4 + 2H_2O \rightarrow Mg(OH)_2 + CaSO_4 \cdot 2H_2O \quad (3)$$

$$Ca(OH)_2 + SO_4^{2-} + 2H_2O \leftrightharpoons CaSO_4 \cdot 2H_2O + 2OH^- \quad (4)$$

The diffraction intensity of $Ca(OH)_2$ in the cathode for the three electrical field groups was EFC > EFN > EFM. Based on chemical Eqs. (3) and (4), the content of $Ca(OH)_2$ was the least in EFM because chemical reaction (3) largely consumes it. The content of $Ca(OH)_2$ was the greatest in EFC due to the abundance of $CaSO_4$, which induced the reversible chemical reaction (4) to shift to the left. The comparison of EFM and M in Fig. 11 shows that the content of $Ca(OH)_2$ in EFM is lower than that of M, indicating that the electrical field could accelerate chemical reaction (3) to quickly expend $Ca(OH)_2$.

The pH of cement-based materials will become increasingly lower as it continues to quickly generate $Mg(OH)_2$, and the presence of $MgSO_4$ leads to the decomposition of ettringite in reaction (5) [29,30]. Thus, there were no characteristic peaks of ettringite in the cathodes of EFM or M in Fig. 11, while thaumasite was discovered.

$$3CaO \cdot Al_2O_3 \cdot 3CaSO_4 \cdot 32H_2O + 3MgSO_4 \rightarrow 4CaSO_4 \cdot 2H_2O + 3\,Mg(OH)_2 + Al(OH)_3 \quad (5)$$

Moreover, $MgSO_4$ will replace Ca^{2+} in the C-S-H gel to generate M-S-H [29], as shown in chemical reaction (6).

$$3CaO \cdot 2SiO_2 \cdot 3H_2O + 3MgSO_4 + 6H_2O \rightarrow 3CaSO_4 \cdot 2H_2O + 2(MgO \cdot SiO_2 \cdot H_2O) + Mg(OH)_2 \quad (6)$$

The chemical Eqs. (3) and (5) generate $Mg(OH)_2$, which will accelerate the decomposition of the C-S-H gel according to chemical kinetics (7) [29].

$$C-S-H + 2H_2O + SO_4^{2-} \rightarrow Ca-depletedC-S-H(oramorphoussilica) + CaSO_4 \cdot 2H_2O \quad (7)$$

The C-S-H gel will combine carbonate and sulfate to generate thaumasite under the above conditions ((8) and (9)) [29,31]. It can be seen in Fig. 11 that the diffraction peak intensity of $CaCO_3$ is the lowest in the cathode of EFM because $CaCO_3$ is exhausted to generate thaumasite.

$$Ca_3Si_2O_7 \cdot 3H_2O + 2MgSO_4 + 2CaCO_3 + Ca(OH)_2 + 28H_2O \rightarrow Ca_6[Si(OH)_6]_2 \cdot [(SO_4)_2 \cdot (CO_3)_2] \cdot 24H_2O + 2Mg(OH)_2 \quad (8)$$

$$6Ca^{2+} + 2SO_4^{2-} + 2CO_3^{2-} + 2[Si(OH)_6]^{2-} + 24H_2O \rightarrow Ca_6[Si(OH)_6]_2 \cdot [(SO_4)_2 \cdot (CO_3)_2]24H_2O \quad (9)$$

In the anode of EFM, there are other corrosion reaction processes (chemical Eq. (2)). H_2O was electrolyzed to H^+. The acidic anode

Fig. 7. Appearance of the four groups after 90 days.

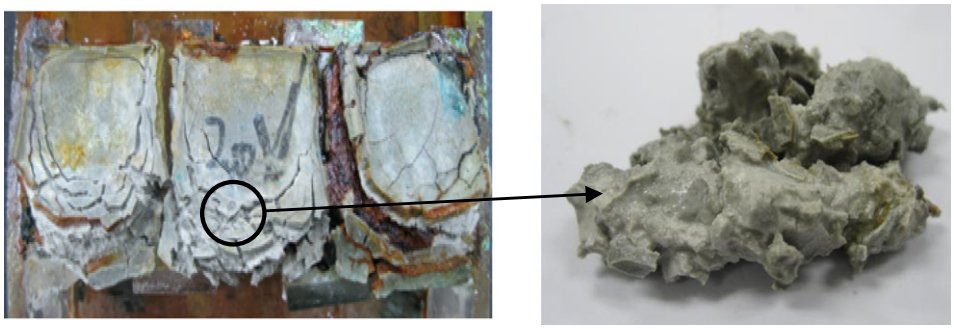

Fig. 8. Appearance of EFM after 120 days.

solution acidized the sample to free Ca^{2+}, which combined with SO_4^{2-} to form gypsum on the anode surface of the sample (Fig. 12). There were two opposite effects in the anode of the sample: (1) SO_4^{2-} migrated from cathode to anode via the electrical field; (2) SO_4^{2-} diffused from the anode solution to the sample via a concentration gradient between the anode solution and the sample. The above two effects (migration and diffusion) were synergistic effects in the cathode [25]. Therefore, abundant SO_4^{2-} ions accumulated in the cathode to consume $Ca(OH)_2$ and form gypsum, while little SO_4^{2-} accumulated in the anode, leading to the peaks of gypsum being lower and the peaks of $Ca(OH)_2$ being higher in the anode than in the cathode in Fig. 13. Meanwhile, Mg^{2+} migrated from the anode solution to the cathode, arriving at the cathode surface of the sample to begin chemical reactions (3) to (9). SO_4^{2-} ions did not persistently migrate from cathode to anode due to the abundance of SO_4^{2-} accumulated in the cathode to form gypsum, ettringite and thaumasite, which jam the pores of the sample. So the corrosion process happened in cathode while not happen in anode.

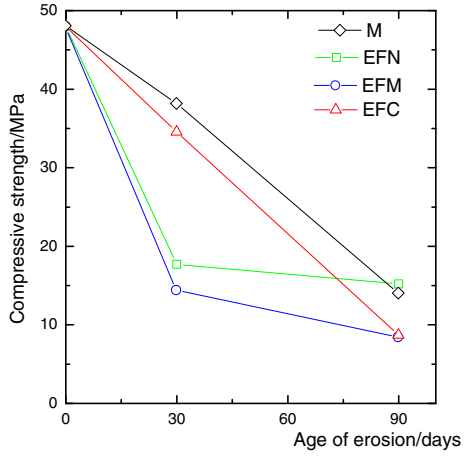

Fig. 9. Compressive strengths of samples after corrosion of 90 days.

From the comparison for EFM in Figs. 11 to 13, TSA quickly occurs in the cement-based materials and generate large amounts of $CaSO_4$. The mechanism is as follows: SO_4^{2-} and Mg^{2+} quickly migrate into the cement-based materials under the electrical field and use $Ca(OH)_2$ for chemical Eq. (3) until $Ca(OH)_2$ is exhausted, as shown by the main diffraction peaks of $Ca(OH)_2$ disappearing in Fig. 13. Meanwhile, the presence of $Mg(OH)_2$ leads to the decline of pH and reduces the stabilization of the C-S-H gel. At the same time, it accelerates the decomposition of the C-S-H gel due to chemical kinetics and generates an abundance of $CaSO_4$ as shown in chemical Eqs. (3), (5), (6) and (7), which reacts with carbonate to form thaumasite that causes TSA.

3.5. FTIR and Raman spectroscopic

FTIR spectra are obtained to confirm the TSA formation of the damaged surface, and the test results are shown in Fig. 14. The FTIR samples were taken from the cathode surface of the four groups. The results show that $[SO_4]$ (1123 cm^{-1}) and $[CO_3]$ (1427 cm^{-1}, 875 cm^{-1}) are discovered in the four test groups due to the sulfate from the external environment and the slurry mixed with $CaCO_3$. $[Si(OH)_6]^{2-}$ is the characteristic peak of thaumasite describing silicon being coordinated with 6 hydroxyls; its peaks are 500 cm^{-1}, 669 cm^{-1}, and 750 cm^{-1}, corresponding to the bending vibration and stretching vibration of $[Si(OH)_6]^{2-}$. There is no thaumasite in the M and EFN groups from peak analysis, while in EFM, there exists typical thaumasite peaks (669 cm^{-1}, 499 cm^{-1}) indicating that it is eroded by TSA. Meanwhile, there is also a thaumasite peak (499 cm^{-1}) in EFC, but it is only a single peak which is not enough to affirm the presence of thaumasite.

Fig. 15 shows the FTIR test results of the pulp from EFM after 120 days. $[Si(OH)_6]^{2-}$ is obviously present, which affirms the formation of thaumasite in agreement with the SEM/EDS and XRD results. Raman spectroscopy gives further confirmation of the presence of thaumasite in Fig. 16. The six Raman spectrum peaks, i.e., 1076, 990, 658, 479, 453, and 417 cm^{-1}, are consistent with the published Raman spectroscopic data for synthetic thaumasite in [32] and [33]. Therefore, it can be affirmed that TSA occurs in the cathode of EFM.

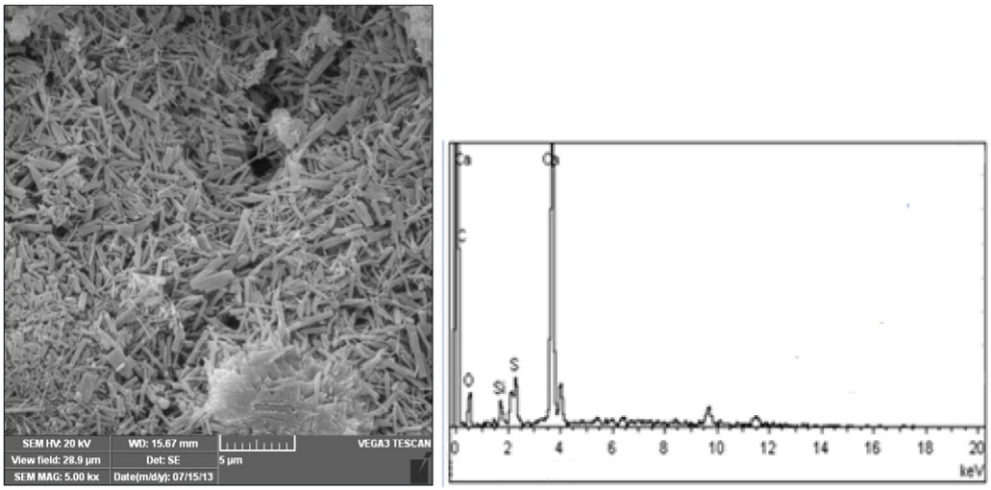

Fig. 10. SEM/EDS profiles of EFM under electrical field attack for 120 days.

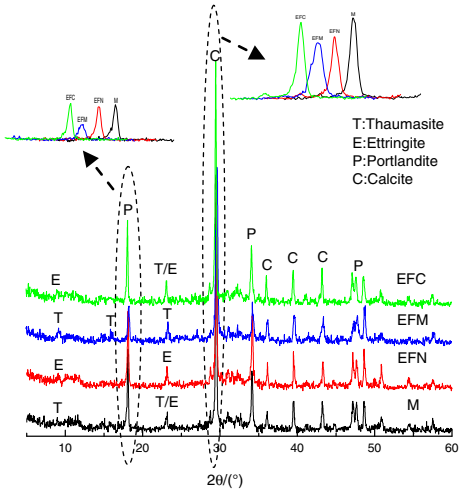

Fig. 11. XRD profiles of samples under the electrical field after 90 days.

The above results show that TSA easily occurs in the EFM condition for the following reasons. The $MgSO_4$ solution is weakly acidic and can therefore generate large amounts of H^+ by electrolyzation, and the H^+ migrates into cement samples under the action of the electrical field from the anode, causing $Ca(OH)_2$ and $Mg(OH)_2$ to lose stability in the cement and form free Ca^{2+} and Mg^{2+}, which migrate to the cathode of the cement samples. Moreover, the H^+ in the anode causes $CaCO_3$ to generate Ca^{2+} ions, which also migrate to the cathode. Additionally, SO_4^{2-} and OH^- migrate into the cement samples in the cathode from the cathode corrosion solution. A significant amount of $CaSO_4$ is present when SO_4^{2-} ions meet Ca^{2+} ions under a high concentration of OH^-, according to the literature [31]. Thus, $CaSO_4$ is present in the cathode under the electrical field. Moreover, the C-S-H gel loses stability when Mg^{2+} is present, and C-S-H reacts with $CaSO_4$ and carbonate to form thaumasite. When the anode solution is Na_2SO_4, the anode and cathode solutions are both neutral; thus, no H^+ ions migrate into the cement in the anode to free Ca^{2+} the cathode. When the anode solution is $CaSO_4$, the anode solution is weakly acidic, freeing Ca^{2+} ions to the cathode. More Ca^{2+} migrates into the cement from the anode solution until there are enough Ca^{2+} ions within the cement to produce more $CaSO_4$. However, the C-S-H is more stable without Mg^{2+}, so it cannot produce a significant amount of thaumasite. The $MgSO_4$ solution ionizes a small amount of H^+ when the immersion method is used, and more free Mg^{2+} ions migrate into the cement samples, reacting with $Ca(OH)_2$ to produce $Mg(OH)_2$, which reduces the stability of C-S-H. However, the migration rate of the ion is much slower than the electrical field, and there is not enough H^+ to free more Ca^{2+} and reduce the pH of the cement; thus, thaumasite cannot be quickly generated.

4. Conclusions and discussion

The present work investigated the effect of an electrical field on the TSA of cement-based materials. The results indicated that the electrical field can quickly accelerate the TSA process in the cathode area of cement-based materials when using Na_2SO_4 solution as the cathode and $MgSO_4$ solution as the anode.

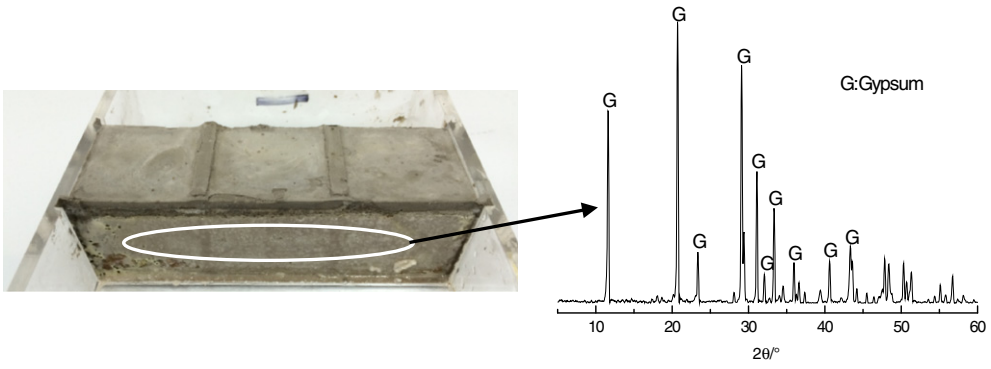

Fig. 12. Reaction sediment on the anode surface.

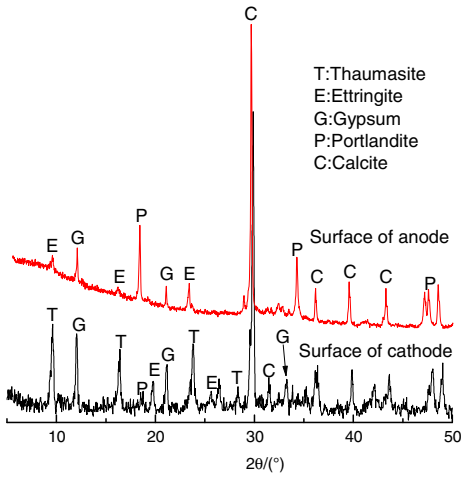

Fig. 13. XRD profiles of EFM under the electrical field for 120 days.

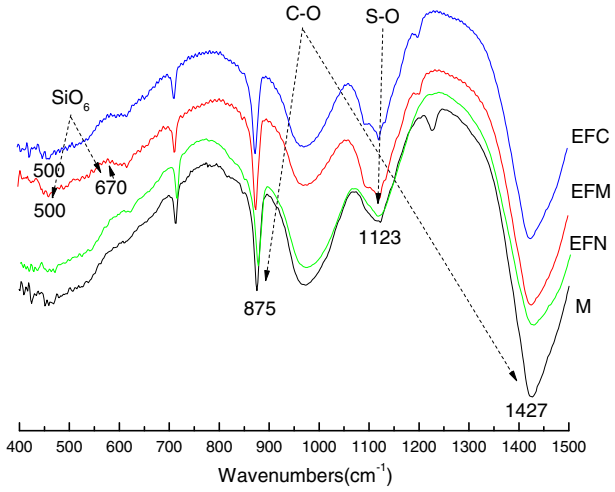

Fig. 14. FTIR spectra of samples under the electrical field for 90 days.

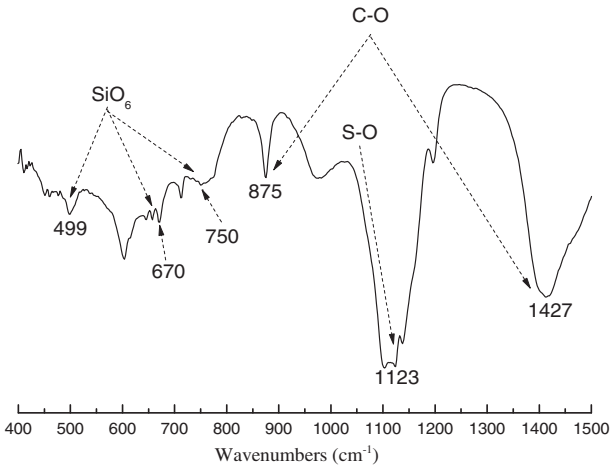

Fig. 15. FTIR spectra of EFM under the electrical field for 120 days.

(1) The results of SEM/EDS, XRD, and FTIR indicated that TSA clearly occurred due to the function of the $MgSO_4$ solution and electrical field after 120 days.

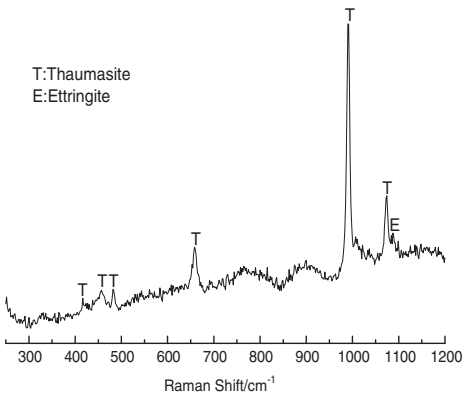

Fig. 16. Raman spectra of EFM under the electrical field for 120 days.

(2) Cement-based materials were more easily damaged by sulfate under an electrical field, which led to noteworthy reduction of compressive strength (particularly when the anodic solution was $MgSO_4$, indicating that the electrical field accelerated TSA).
(3) The electrical field mainly accelerated the migration of ions into the cement-based materials and the rates of the chemical reactions in the cement-based materials.

However, more research is required on the mechanism of TSA under the action of electrical fields, especially the ion distribution (Ca^{2+}, Mg^{2+}, and SO_4^{2-}) and pH at different sites in cement-based materials. Moreover, different electric field parameters should be researched in the future, e.g., electrical field voltage and electrical field period.

Acknowledgments

The authors want to acknowledge the financial support of the National Natural Science Foundation of China (No. 51572038).

References

[1] L. Lin, X. Zhou, Experimental study on metro stray current corrosion of rebars in reinforced concrete and the influence of corrosion on concrete strength, Tunnel 6 (1999) 1–8 (In Chinese).
[2] V. Hock, S. Morefield, J.B. Bushman, Evaluating the performance of the electro-osmotic pulse basement dewatering system, Mater. Perform. 1 (2006) 24–28.
[3] V. Hock, S. Morefield, M. Mcinerney, et al., Control of water migration through concrete using electro-osmosis, Mater. Perform. 7 (2005) 42–47.
[4] W. Gan, M. Gao, Effects of stray current on reinforced concrete durability, Concrete 6 (2009) 21–24 (In Chinese).
[5] P. Zhan, Research of the Influence of Metro Stray Current Corrosion on Reinforced Concrete Structures and Protection, Beijing Jiaotong University, 2009 (In Chinese).
[6] J. Gen, The Research on the Deteriorated Mechanisms of Reinforced Concrete in Stray Currents and Chloride Ion Coexisted Corrosion Environment, Wuhan University of Technology, 2008 (In Chinese).
[7] L. Bertolini, M. Carsana, P. Pedeferri, Corrosion behaviour of steel in concrete in the presence of stray current, Corros. Sci. 49 (2007) 1056–1068.
[8] S. Diamond, Thaumasite in Orange County, Southern California: an inquiry into the effect of low temperature, Cem. Concr. Compos. 25 (2003) 1161–1164.
[9] M.E. Gaze, N.J. Crammond, The formation of thaumasite in a cement:lime:sand mortar exposed to cold magnesium and potassium sulfate solutions[J], Cem. Concr. Compos. 22 (2000) 209–222.
[10] M. Amareanu, L. Melita, Aspects of improving concrete durability, Stud. Univ. Babes-Bolyai Chem. 2 (2014) 7–16.
[11] M. Fenchel, H.S. Mueller, Sulfate attack on concrete-mechanisms and prediction model, in: W. Brameshuber (Ed.), RILEM Proceedings, 76, 2010, pp. 229–238.
[12] M. Hu, M. Tang, A summary of the research on thaumasite form of sulfate attack, Concrete 6 (2004) 17–19 (In Chinese).
[13] D. Deng, J. Xiao, Q. Yuan, et al., On thaumasite in cementitious material, J. Build. Mater. 4 (2005) 400–409 (In Chinese).
[14] C. Shi, D. Wang, A. Behnood, Review of thaumasite sulfate attack on cement mortar and concrete, J. Mater. Civ. Eng. 12 (2012) 1450–1460.
[15] T.A. Johnson, M. Tomik, G.M. Bowers, Kinetics of the thaumasite form of sulfate attack on cement and concrete, Abstr. Pap. Am. Chem. Soc. (2012) 243.
[16] E. Freyburg, A.M. Berninger, Field experiences in concrete deterioration by thaumasite formation: possibilities and problems in thaumasite analysis, Cem. Concr. Compos. 25 (2003) 1105–1110.

[17] J. Bensted, Thaumasite-direct, woodfordite and other possible formation routes, Cem. Concr. Compos. 25 (2003) 873–877.
[18] J. Aguilera, S. Martínez-Ramírez, I. Pajares-Colomo, et al., Formation of thaumasite in carbonated mortars, Cem. Concr. Compos. 25 (2003) 991–996.
[19] C. Li, Y. Yao, L. Wang, Accelerate thaumasite form of sulfate attack in cement-basted materials by internal doping magnesium sulfate, J. Chin. Ceram. Soc. 7 (2010) 1197–1200 (In Chinese).
[20] Y. Luo, The Study of Accelerate TSA Using Electro Pulse, Chongqing university, Chongqing, 2014 (In Chinese).
[21] D.W. Hobbs, Thaumasite sulfate attack in field and laboratory concretes: implications for specifications[J], Cem. Concr. Compos. 25 (2003) 1195–1202.
[22] Z. Liu, D. Deng, G. De Schutter, et al., The effect of $MgSO_4$ on thaumasite formation, Cem. Concr. Compos. 35 (2013) 102–108.
[23] S. Tsivilis, K. Sotiriadis, A. Skaropoulou, Thaumasite form of sulfate attack (TSA) in limestone cement pastes, J. Eur. Ceram. Soc. 27 (2007) 1711–1714.
[24] A. Skaropoulou, S. Tsivilis, G. Kakali, et al., Thaumasite form of sulfate attack in limestone cement mortars: a study on long term efficiency of mineral admixtures, Constr. Build. Mater. 23 (2009) 2338–2345.
[25] C. Wang, Y. Luo, Y. Chao, Behavior and mechanism of sulfate attack in cement based materials by action of electrical pulse, J. Hunan Univ. 12 (2014) 40–46 (In Chinese).
[26] S. Lorente, M.-P. Yssorche-Cubaynes, J. Auger, Sulfate transfer through concrete: migration and diffusion results[J], Cem. Concr. Compos. 33 (2011) 735–741.
[27] Q. Huang, C. Wang, Q. Zeng, et al., Deterioration of mortars exposed to sulfate attack under electrical field, Constr. Build. Mater. 117 (2016) 121–128.
[28] Q. Huang, C. Wang, C. Yang, et al., Accelerated sulfate attack on mortars using electrical pulse, Constr. Build. Mater. 95 (2015) 875–881.
[29] X. Jia, T. Wu, Q. Guo, et al., Effects of $MgSO_4$ on thaumasites formation, Concrete 11 (2014) 70–74 (In Chinese).
[30] M. Santhanam, M.D. Cohen, J. Olek, Sulfate attack research-whither now, Cem. Concr. Res. 31 (2001) 845–851.
[31] S.A. Hartshorn, J.H. Sharp, R.N. Swamy, Thaumasite formation in Portland-limestone cement pastes, Cem. Concr. Res. 29 (1999) 1331–1340.
[32] L. Gao, D. Xuegang, L. Kong, Quantitative analysis of effect of limestone powder on resistance of thaumasite attack to cement-based materials, J. Southeast Univ. (Nat. Sci. Ed.) 3 (2012) 483–487 (In Chinese).
[33] R. Yang, N.R. Buenfeld, Microstructural identification of thaumasite in concrete by backscattered electron imaging at low vacuum, Cem. Concr. Res. 30 (2000) 775–779.